Malaysian NANO-An International Journal

Research Article

Received 10th June 2021
Revised 28th July 2021
Accepted 12th August 2021

DOI:
https://doi.org/10.22452/mnij.vol1no1.6

Corresponding author:
jeyanthinath.chem@mkuniversity.org

Microwave-Assisted Synthesized Gadolinium Doped Barium Strontium Titanate Nanostructures: Structural and Optical Properties for DSSC Applications

V. Kavitha[1], V. Ragavendran[2], N. Sethupathi[1], Suresh Sagadevan[3], V. Sasirekha[4], J.M. Pearce[5] and Jeyanthinath Mayandi[2]*

[a]*Department of Physics, Arignar Anna Government Arts College, Namakkal-637002, Tamil Nadu, India.*
[b] *Department of Materials Science, School of Chemistry, Madurai Kamaraj University, Madurai-625 021, India.*
[c]*Nanotechnology and Catalysis Research Centre, University of Malaya, 50603, Kuala Lumbur, Malayasia.*
[d]*Department of Physics, Avinashilingam Institute for Home Science and Higher Education for Women, Coimbatore, India*.
[e]*Department of Electrical and Computer Engineering, Western University, London, ON, Canada*

Abstract

Gadolinium (Gd) doped barium strontium titanate (BST) was prepared using the microwave-assisted solid-state reaction method for dye sensitized solar cell (DSSC) applications. The optical properties and the structural analysis of the prepared samples reveal the optical band gap and the morphology. The XRD pattern of the annealed samples confirms the polycrystalline nature with the cubic crystal structure. When the dopant is added, the bandgap increases slightly from 3.11 to 3.27 eV. The J-V characteristics of DSSCs prepared with pure and doped BST were investigated. The efficiency of the DSSCs remained constant and there is a slight increase in the Jsc for highly doped samples under 1-sun illumination. Gadolinium doped barium strontium titanate shows variation in the J-V characteristics and could be a potential candidate for the solar photovoltaic applications.

***Keywords*:** Barium strontium titanate, Gadolinium. Microwave synthesis, Dye sensitized solar cell, Photovoltaic

1. Introduction

Although the levelized cost of electricity from solar photovoltaic (PV) technologies [1] is so low that it is forcing fossil fuels off the grid [2], there is a concerted effort to increase PV deployment velocity and reach the terra watt scale [3]. The current PV industry is dominated by silicon-based PV [4]. Although silicon-based PV is still undergoing a rapid learning curve [5,6] and has new technological improvements being scaled up that reduce costs like black silicon [7,8] it is still fundamentally limited by a relatively low single bandgap of 1.12eV [9]. One approach to further driving down PV costs and accelerating PV adoption is to transition to non-silicon-based PV [10, 11]. Ternary metal oxides are considered a potential candidate for PV devices due to their high bandgap energy [12]. Among different types of metal oxides, strontium titanate ($SrTiO_3$) has more structural similarities with anatase titanium dioxide (TiO_2) [13], which is the conventional material for dye-sensitized solar cells (DSSCs) [14]. Sr atoms can be replaced with Ba to form $BaSrTiO_3$ (BST) with modified crystalline structure and properties [15]. BST is a useful electronic material because of its high electric permittivity and dependence of Curie temperature on its composition, utilized with a large number of applications in the manufacture of thermistors, multilayer capacitors, electro-optical devices and semiconductor devices, tunable filter and antenna devices, capacitor devices and other applications [12]. Suitably tuning bandgap, $BaSrTiO_3$ can be made as a promising material for the development of DSSCs to yield higher open-circuit voltage (V_{OC}) values [16]. A dye-sensitized solar cell of $SrTiO_3$ offers a high open-circuit voltage compared with TiO_2, due to the reduction in recombination loss leads to an increase in electron transport. By doping or substitution of atoms into Ba or Sr sites, the band structure and its electrical properties are easily controlled [17]. BST has higher stability, tunability, and low optical losses [18]. Many methods have been developed to prepare the material, the most common of which are based on sol-gel and hydrothermal technologies [19]. Rare-earth ions doped BST can enhance the thermal and electro-optical properties. Both the mechanism and luminescence properties on erbium-doped $Ba_{0.65}Sr_{0.35}TiO_3$ nanocrystals were reported by Wang et al., [20]. Manganese and yttrium co-doped BST ceramics prepared through the citrate nitrate combustion method are investigated by Zunping and Hua [21]. To improve the electrical and dielectric properties of BST, Reenu et al., [22] followed the solid-state reaction method for preparing Fe doped BST. La_2O_3 doped barium strontium titanate ceramics for capacitor applications is demonstrated by Chen et al., [23] using the solid-state reaction method. Niobium doped $Ba_{0.25}Sr_{0.75}TiO_3$ semiconductor thin

films are studied by Setiawan et al., [24] and concluded BST acts as a photodiode with respect to the addition of dopant.

To build on this work, which have demonstrated that the properties of BST can be altered for a range of application from doping, this study uses low-cost industrially scalable processes in order to investigate for the first-time gadolinium-doped BST nanostructures. In order to provide a scalable synthesis method, BST was prepared in here using a simple apparatus and inexpensive reagents. The microwave-assisted solid-state reaction is investigated to fabricate BST with three different gadolinium dopant concentrations at low temperatures. The effect of gadolinium doped BST on structural, electrical, and optical properties were studied in-depth and compared to pure BST nanostructures on both the material level and for DSSC applications.

2. Experimental details

2.1 Synthesis of Gadolinium Doped Barium Strontium Titanate nanostructures

The materials used in the process are barium acetate (C4H6BaO4 - 99.99%), Strontium acetate C4H6O4Sr - 99.995%), titanium (IV) dioxide (TiO2), Gadolinium (III) nitrate hexa hydrate (Gd 3 (NO3) · 6H2O), are purchased from Sigma-Aldrich. Sample of compositions Ba0.5Sr0.5 (Ti1-xGdxO3); x = 0.0, 0.2, 0.4 and 0.6 were prepared using the microwave-assisted solid-state reaction method. The stoichiometric proportions of the starting materials were weighed and mixed with an agate mortar and pestle. After 15 min of grinding, 25mL of Double distilled (DD) water was added to it and then stirred 5 min to get a homogeneous solution of precursor material. The above solution was kept in a domestic model microwave oven of 2450 MHz frequency with 1250 Watt for 30 min. During the microwave process, the precursors reacted together. The resulting pale green color solution was dried in a hot air oven at 120°C for 24 h and then kept overnight to dry. The powder was collected and calcined for two hours in a muffle furnace at 800°C. Following the calcination process, the powders were ground for 30 minutes to obtain fine BST and Gd doped BST powders.

2.2 Instrumental analysis

Morphological features of pure and Gd-doped BST were studied using FESEM (Zeiss18 Evaluation). XRD measurement was done using Rigaku Miniflex X-ray diffractometer equipped with CuKα (λ = 1.54 Å)). Diffused reflectance spectra for the prepared samples were characterized

using a setup consisting of DH- 2000 BAL Ocean Optics light source to generate light in the visible and ultra-violet regions. An Ocean optics USB 4000 detector is used to collect the diffused reflected spectrum.

2.3 Photovoltaic (PV) Cell Fabrication

The BSGT photoanode was prepared using the doctor blade method for a 5 mm x 5mm area on ITO (12Ω/Sq.cm) and immersed in 0.5mM of N719 dye in anhydrous ethanol for 16 hours at room temperature. The platinum counter electrode was made by drop-casting a chloroplatinic acid solution onto the substrate, which was sintered at 450°C for 30 minutes. The dye incorporated BSGT working electrode and Pt counter electrode was fabricated using the conventional DSSC method [17].

The electrolyte solution was made by combining acetonitrile, 4-tert-butyl pyridine, lithium iodide (LiI), and iodine (I_2) in the following molar ratios: 0.3:0.5:0.05. The electrolyte solution was injected between the two electrodes. Photocurrent-voltage (I-V) measurements of DSSCs were carried out using (Photoemission tech, USA) PET AAA grade solar simulator with Keithley 2400 source meter under sun illumination (AM 1.5) 100mW/cm^2. I-V and electrochemical measurements were performed in an open-cell configuration.

3. Results and discussions

3.1 Surface morphological Properties

FESEM image analysis reveals that microwave treatment of BST leads to the formation of agglomeration of particles. Figure 1 shows the FESEM images of the prepared pure and Gd-doped BST nanostructures with different concentrations of dopant. In Figure 1, for pure BST and higher concentration of Gd content in BST it showed agglomerated particles. The FESEM images of undoped BST (Figure 1(a)) revealed that the particles were aggregated and that the particle size was in the 100 nm range. Figure 1(b) shows the FESEM image of BSGT(x=0.2), which revealed that particle sizes were in the range of 80 nm. The FESEM image of BSGT (x=0.4) is shown in Figure 1(c). According to the FESEM images, the particles are spherical. The FESEM image BSGT (x=0.6) Figure 1(d) revealed that these spherical particles were joined together to form a sponge like structure. Increasing the dopant concentration in BST has the microwave particles formed in a spherical shape and then coalescence. This may be due to the dopant entered into the lattice of BST that alters the crystallinity and shape. Most of the particles presented with a size of

around 100 nm. The morphology exhibits that the narrower particle distribution on the surface of Gd doped BST nanostructures. The very close and tightly packed particles on surface morphologies support the efficient formation of charge carriers [24].

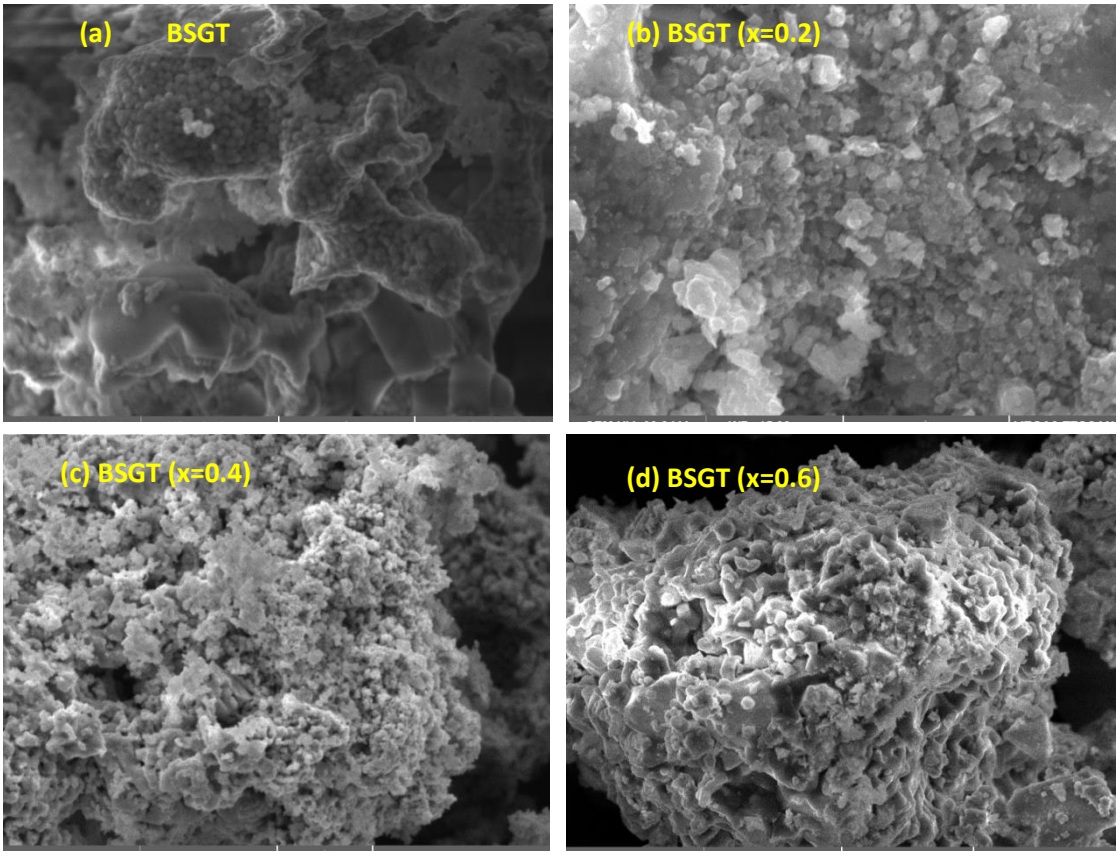

Figure.1 FESEM images of Gd doped BST (x = concentration of the dopant Gd in BST) (a) BSGT (x=0.0), (b) BSGT (x=0.2), (c) BSGT (x=0.4) and (d) BSGT (x=0.6).

3.2 Structural Analysis

The powder X-ray diffraction (XRD) pattern of annealed BST and Gd-doped BST samples prepared with different concentrations of Gd content under the same processing parameters is shown in Figure 2. The prepared powders were found to be crystalline in nature. The diffraction peaks observed at 22.4°, 32.1°, 39.6°, 45.9°, 57.2°, and 67.2° are attributed to the (100), (110), (111), (200), (211), and (220) diffraction planes of cubic structured BST in the Pm3/m space group and compared with JCPDS card No. 39-1395. The crystallite size of the prepared BST sample was calculated to be 44.61 nm using Debye Scherrer's formula. The diffraction peaks with varying intensities observed for the Gd doped BST at 27.2°, 28.6°, 38.1°, and 44.3° correspond to the (100), (110), (111), and (400) planes. Diffraction peaks shifted in Gd doped concentrations x=0, 0.2, 0.4,

and 0.6 with BST. The crystallite size for Gd doped BST samples x=0.2, 0.4, and 0.6 was calculated to be 42.73, 41.04, and 38.86 nm, respectively. It was also found that as Gd concentration in BST increased, the intensity of the peak corresponding to the (110) plane decreased.

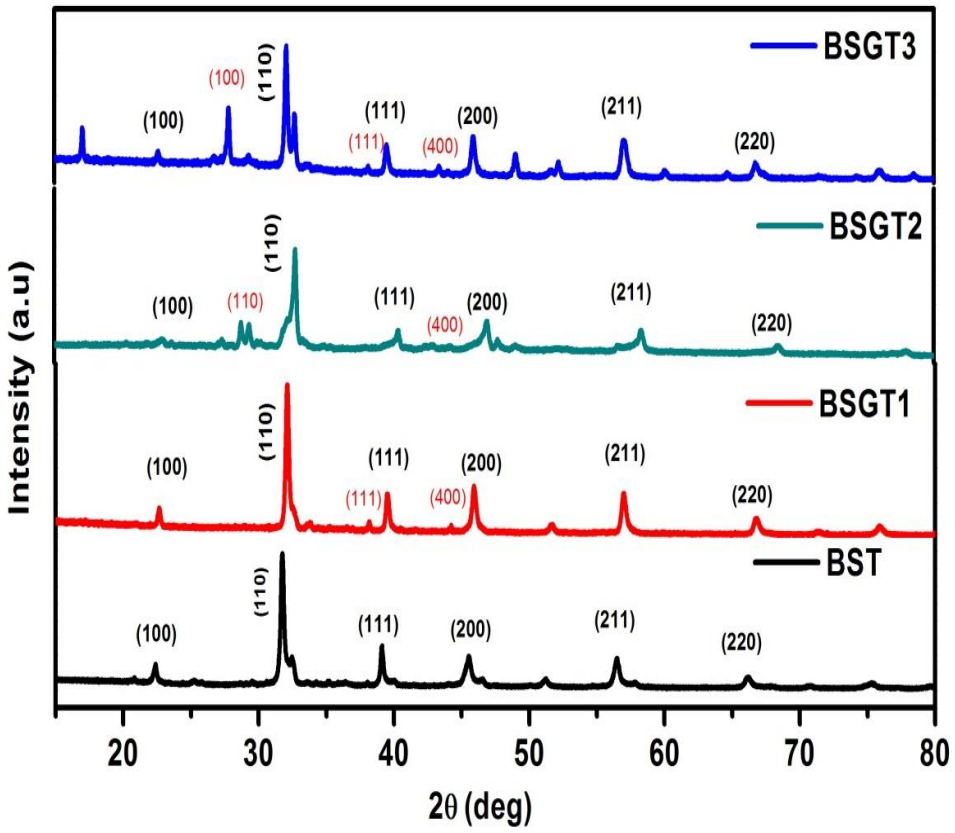

Figure.2 Powder XRD patterns of pure and Gd doped BST nanostructures.

The shift of XRD peaks towards a higher angle for BSGT2 sample indicates the crystal lattice is compressed [17]. The peaks shifted towards a lower angle for BSGT3 indicates the lattice was expanded. These facts can be attributed to the changes in the stoichiometric composition of Gd. The smaller ionic size of Gd reduced the crystal lattice strain at doping concentration BSGT2 (x=0.4). However, with increasing doping concentration of Gd to x=0.6, the enlargement of crystal lattice occurs mainly due to the dominance of stoichiometric factor rather than ionic size factor [25].

3.3 Optical Properties

Figure 3 (a) depicts the diffuse reflectance spectra of pure and different concentrations of Gd doped BST nanopowders. The Kubelka-Munk function can be used to relate the absorption coefficient (k) to the reflectance (R) [26]. The absorption spectra are shown in Figure 3(b) after being translated from diffuse reflectance using the Kubelka -Munk function F(R). The modified Kubelka–Munk function can be used to calculate the sample's bandgap (Eg). Figure 3(c) and (d) show the direct and indirect band gaps of pure and Gd doped BST nanostructures, respectively. The prepared samples BST, BSGT1, BSGT2, and BSGT3 have indirect energy bandgaps of 3.11, 3.24, 3.13, and 3.27 eV, respectively. The pure BST bandgap is slightly lower than that of the Gd doped samples. The observation is consistent with XRD and FESEM analysis, which show that when a dopant is added, the particle size decreases.

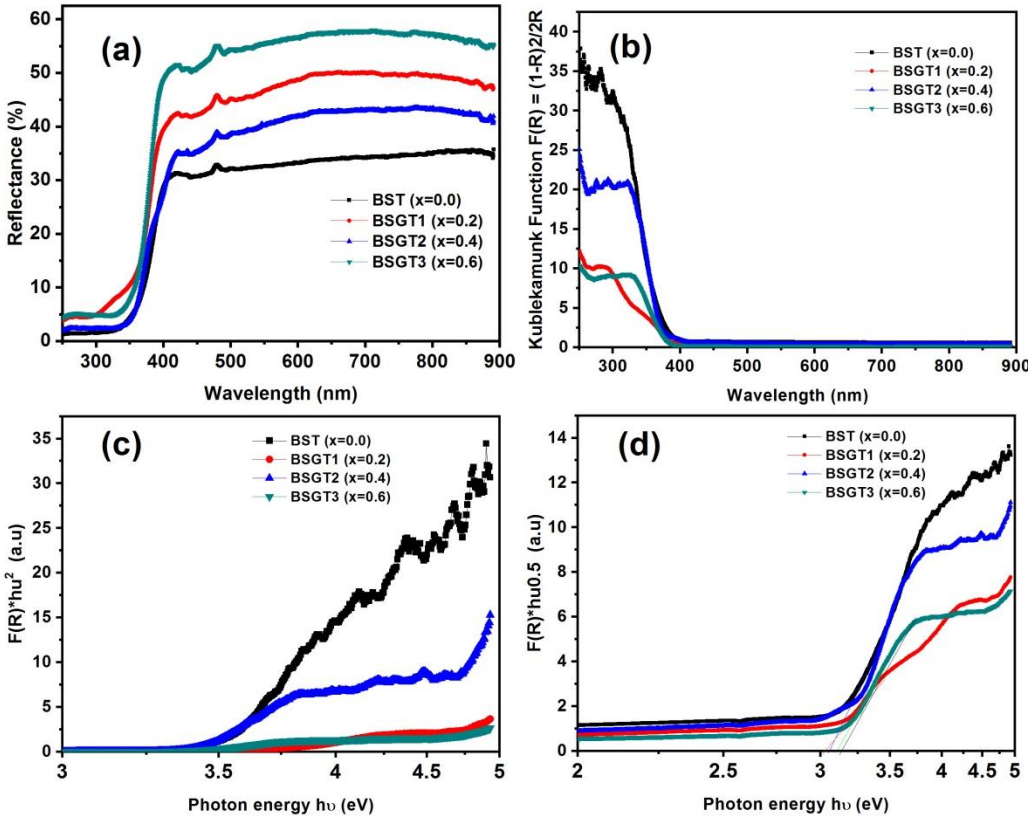

Figure. 3 UV-VIS spectroscopy of analysis of pure and Gd-doped BST nanopowders by DRS method (a) reflection spectra, (b) the absorbance spectrum Function (c) the direct bandgap, and (d) indirect bandgap calculated from modified Kublelka Munk Function

4.4 *J-V Characteristics for DSSCs*

The J-V characteristics of the DSSCs made with all of the undoped and Gd-doped BST materials show that all of the samples had diode properties. The current density and voltage curve for undoped and Gd-doped BST DSSC is shown in Figure 4. Table 1 summarizes the bandgap, crystallite size, I-V characteristics, and conversion efficiency of BST, BSGT1, BSGT2, BSGT3. Under standard global AM 1.5 solar irradiation, the prepared solar cell sensitized with N719 dye gave a short circuit current density (J_{SC}) of 0.73mA/cm^2, open-circuit voltage (V_{OC}) of 0.57 mV, corresponding to overall conversion efficiency (η) of 0.28%.

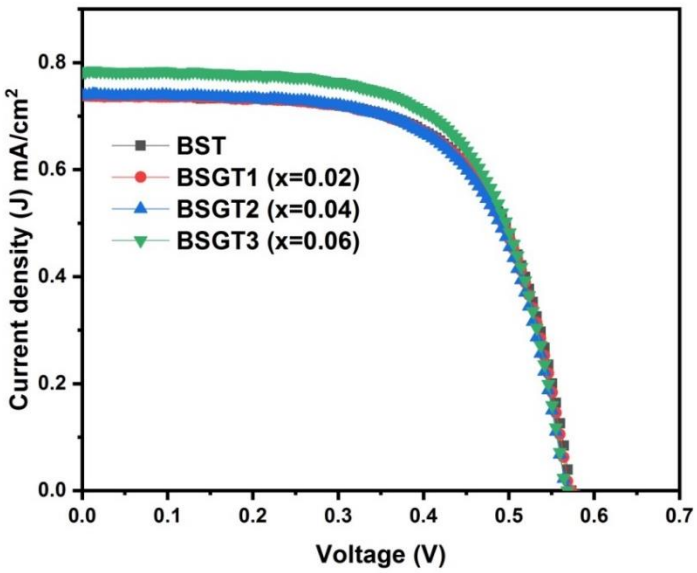

Figure. 4 Current density (J) and voltage (V) characteristics of pure and Gd-doped BST nanostructures.

On reaching the breakdown voltage, there was no change in the current density for samples with various doping concentrations. Doping causes more free electrons and holes to be liberated in the crystal [27]. Free electrons in the samples increase the conduction. The occurrence of conductive properties is due to the photon energy absorbed by the electron.

Table 1: The bandgap, crystallite size, and photovoltaic parameters of BST and Gd-doped BST

Parameters	**BST**	**BSGT1**	**BSGT2**	**BSGT3**
Band gap (eV)	3.11	3.24	3.13	3.27
Crystallite size(nm)	44.61	42.73	41.07	38.06
J_{sc} (mA/cm^2)	0.73	0.73	0.74	0.78
V_{oc} (V)	0.57	0.57	0.57	0.57
FF	0.65	0.65	0.64	0.64
Efficiency	0.27	0.27	0.27	0.28

4. Conclusions

This study has demonstrated a simple and cost-effective microwave-assisted solid-state reaction method to synthesis pure and Gd-doped barium strontium titanate nanoparticles. The FESEM images show the particles are agglomerated and spherical. The XRD pattern of the annealed samples revealed the polycrystalline nature with the cubic crystal structure. There is also observed slight increase in the bandgap when BST is doped with Gd from about 3.1eV to about 3.2eV regardless of concentration of the dopant. The efficiency of the solar cell remains constant and there is a slight increase in the Jsc for highly doped (x=0,6) samples. Future work is needed to improve the performance of the DSSCs to be competitive with more established technologies.

Conflict of interest

The authors declare no conflict of interest with this work.

Acknowledgement

JM&VR acknowledges the support of UGC-UPE, DST-PURSE&FIST and MKU. This work was supported in part by the Thompson Endowment.

References

[1] K. Branker, M.J.M. Pathak, J.M. Pearce. "A review of solar photovoltaic levelized cost of electricity." *Renewable and sustainable energy reviews*. 2011; 15, 9: 4470-4482.

[2] F. Robert. Service, Giant batteries and cheap solar power are shoving fossil fuels off the grid sciencemag.org, news. 2019; 11, (07)

[3] N.M. Haegel, Jr.H. Atwater, T. Barnes, C. Breyer, A. Burrell, Yet-M.Chiang, S. De Wolf, Terawatt-scale photovoltaics: *Transform global energy, Science*. 2019; 364, 6443: 836-838,

[4] Singh, Rajendra. Why silicon is and will remain the dominant photovoltaic material. *Journal of Nanophotonics.* 2009; 3: 032503.

[5] Metz, A., M. Fischer, and J. Trube. International technology roadmap for photovoltaics (ITRPV): Crystalline silicon technology-current status and outlook. *Proceedings of the PV Manufacturing in Europe Conference, Brussels, Belgium*. 2017

[6] Oberbeck, Lars, Katherine Alvino, Baljeet Goraya, and Marie Jubault. IPVF's PV technology vision for 2030. *Progress in Photovoltaics: Research and Applications*. 2020; 28, no. 11: 1207-1214.

[7] Srivastava, Sanjay K., Prashant Singh, Avritti Srivastava, P. Prathap, Sushil Kumar, C. M. S. Rauthan, and D. K. Aswal. Nanostructured Black Silicon for Efficient Thin Silicon Solar Cells: Potential and Challenges. In Recent Advances in Thin Films. *Springer, Singapore*. 2020; 549-623.

[8] Modanese, Chiara, Hannu S. Laine, Toni P. Pasanen, Hele Savin, and Joshua M. Pearce. Economic advantages of dry-etched black silicon in passivated emitter rear cell (PERC) photovoltaic manufacturing. *Energies 11*. 2018; no. 9: 2337.

[9] Andreani, Lucio Claudio, Angelo Bozzola, Piotr Kowalczewski, Marco Liscidini, and Lisa Redorici. Silicon solar cells: toward the efficiency limits. *Advances in Physics. 2019;* X 4, no. 1: 1548305.

[10] T. Unold, H.W. Schock. "Nonconventional (non-silicon-based) photovoltaic materials." *Annual Review of Materials Research. 2011;* 41: 297-321.

[11] D. Nikolić, B. Milorad, S. Jasmina, R. Jasna, T. Dragan. A review of non-silicon and new photovoltaics technology for electricity generation. *Proceedings of the International Conference on Renewable Energy Sources – MKOIEE*. 2018; 2,1: 1-7.

[12] R. Jose, T. Velmurugan, R. Seeram, Metal oxides for dye sensitized solar cells. *J. Am. Ceram. Soc.* 2009; 92, 2: 289-301.

[13] J.Mayandi, S. Mahalakshmi, V. Ragavendran Optical and structural studies of $BaTiO_3$ and $SrTiO_3$. *Journal of Nano Science and Nano Technology*. 2014; 2: 735-738.

[14] Thomas, Sara, T. G. Deepak, G. S. Anjusree, T. A. Arun, Shantikumar V. Nair, and A. Sreekumaran Nair. A review on counter electrode materials in dye-sensitized solar cells. *Journal of Materials Chemistry.* 2014; A2, no. 13: 4474-4490.

[15] Pai, Yun-Yi, Anthony Tylan-Tyler, Patrick Irvin, and Jeremy Levy. Physics of $SrTiO_3$-based heterostructures and nanostructures: a review. *Reports on Progress in Physics*. 2018; 81, no. 3: 036503.

[16] P. Jayabal, V. Sasirekha, J. Mayandi, K. Jeganathan, V. Ramakrishnan, "A facile hydrothermal synthesis of $SrTiO_3$ for dye sensitized solar cell application". *Journal of Alloys and Compounds*. 2014; 586: 456–461

[17] J. Vinodhini, J. Mayandi, R. Atchudan, P. Jayabal, V. Sasirekha, Effect of microwave power irradiation on TiO_2 nano-structures and binder free paste screen printed dye sensitized solar cells. *Ceramics International, Elsevier*. 2019; 45, 4: 4667-4673.

[18] Y Shen, BST-inspired Smart Flexible Electronics. *Electronic Theses and Dissertations*. 2012; 2483.

[19] R. Pazik, D. Hreniak, W. Strek, A. Speghini, M. Bettinelli, Structural and luminescence properties of Eu_3+ doped BaxSr1-$xTiO_3$ (BST) nanocrystalline powders prepared by different methods. *Optical Materials*. 2006; 28: 1284–1288.

[20] A.W. Nuayi, A. Husin, S.H. Irzaman and R. Mamat,, Enhancement of Photon Absorption on BaxSr1−$xTiO_3$ Thin-Film Semiconductor Using Photonic Crystal. *International Journal of Optics*. 2014; 534145: 1- 8,

[21] Z. Xu, H. Qiang Enhanced electrocaloric effect in Mn + Y co-doped BST ceramics near room temperature, *Materials Letters*. 2017; 191: 57-60

[22] Reenu J, Harikrishnan G N, Jayakumari I. *Processing and Applications of Ceramics*. 2015; 9: 73-79

[23] Z Chen, C Fangxu, L Zhixin, J Gang and L Yuanliang. Microstructure and dielectric properties of La_2O_3 doped Ti-rich barium strontium titanate ceramics for capacitor applications. *Materials Science-Poland*. 2017; 35: 806-815.

[24] A. Setiawan, Aminullah, J. Juansah, Irzaman, Optical and Electrical Characterizations of Niobium-doped $Ba_{0.25}Sr_{0.75}TiO_3$ (BSNT) on p-type Silicon and Corning Glass Substrates and

its Implementation as Photodiode on Satellite of LAPAN – IPB". *Procedia Environmental Sciences*. 2016; 33: 620-625.

[25] M. Selvaraj, R. Venkatesan, J. Mayandi, V. Venkatachalapathy, "Influence of tin (IV) doping on structural and optical properties of rhombohedral barium titanate ($BaTiO_3$)". *Materials Today: Proceedings*. 2019.

[26] R. Venkatesan, J. Mayandi, J.M. Pearce, V. Venkatachalapathy, "Influence of metal assisted chemical etching time period on mesoporous structure in as-cut upgraded metallurgical grade silicon for solar cell application". *J Mater Sci: Mater Electron*. 2019; 30, 9: 8676–8685,

[27] S.H. Xiao, W.F. Jiang, K. Luo, J.H. Xia, L. Zhang, "Structure and ferroelectric properties of barium titanate films synthesized by sol–gel method". *Materials Chemistry and Physics*. 2011; 127; 420–425.